Laser-assisted XUV double ionization of helium: Energy-sharing dependence of joint angular distributions

Aihua Liu and Uwe Thumm

James R. Macdonald Laboratory, Department of Physics, Kansas State University, Manhattan, Kansas 66506-2604, USA

(Received 12 March 2015; published 23 April 2015)

By numerically solving the time-dependent Schrödinger equation in full dimensionality, we discuss the dependance of joint photoelectron angular distributions on the energy sharing of the emitted electrons for the double ionization of helium atoms by ultrashort pulses of extreme ultraviolet (XUV) radiation in coplanar emission geometry with and without the presence of a comparatively weak infrared (IR) laser pulse. For IR-laser-assisted single-XUV-photon double ionization, our joint angular distributions show that the IR-laser field enhances back-to-back electron emission and induces a characteristic splitting in the angular distribution for electrons that are emitted symmetrically relative to the identical linear polarization directions of the XUV and IR pulse. These IR-pulse-induced changes in photoelectron angular distributions are (i) imposed by different symmetry constraints for XUV-pulse-only and laser-assisted XUV double ionization, (ii) robust over a large range of energy sharings between the emitted electrons, and (iii) consistent with the transfer of discrete IR-photon momenta to both photoelectrons from the assisting IR-laser field. While selection-rule forbidden at equal energy sharing, for increasingly unequal energy sharing we find back-to-back emission to become more likely and to compete with symmetric emission.

DOI: 10.1103/PhysRevA.91.043416 PACS number(s): 32.80.Rm, 33.80.Rv, 42.50.Hz

I. INTRODUCTION

Double ionization (DI) of helium atoms by extreme ultraviolet (XUV) pulses from synchrotron radiation sources has been a subject of intense research for more than two decades [1,2]. The first measurement of the triply differential cross section (TDCS) for direct (nonsequential) single-photon double photoionization in helium at equal energy sharing of the emitted electrons was reported by Schwarzkopf *et al.* [3]. The TDCS for single-photon DI at unequal energy sharing was measured subsequently by Schwarzkopf *et al.* [4,5] and Bräuning *et al.* [6]. Due to their extremely small values, the measurement of two-photon DI cross sections has remained a challenge in the laboratory. To the best of our knowledge, the first measured two-photon DI cross sections of helium were published in 2005 by Hasegawa *et al.* [7]. In this experiment, intense high harmonics in the soft x-ray spectral domain were used, and two-photon DI cross sections for XUV pulses with a photon energy of 42 eV were estimated as 4×10^{-53} cm^{4}s.

On the theoretical side, following up on the Wannier theory for the break-up of three Coulomb-interacting particles [8,9], Huetz *et al.* [10] calculated triply and doubly differential cross sections for the DI of helium, focusing on the parametrization and interpretation of angular correlation between the two escaping photoelectrons. Soon afterwards, Briggs and coworkers derived selection rules for helium DI, emphasizing their relevance for the understanding of photoelectron angular distributions [1,11–14]. The convergent close-coupling (CCC) calculations by Keifets and Bray [6], TDCSs calculated by Huetz *et al.* [6,10], as well as TDCSs obtained from time-dependent close-coupling (TDCC) simulations by Palacios *et al.* [15] were found to be in good agreement with the angular distributions in the absolute TDCSs for the DI of helium by 99 eV XUV photons measured by Bräuning *et al.* [6]. Comprehensive numerical studies on the DI of helium following the absorption of a few XUV photons were carried out by Parker *et al.* [16] starting 15 years ago. Following the 2005 experiment of Hasegawa *et al.* [7], two-photon DI of helium has been the subject of several theoretical studies [15,17–28]. In particular, Zhang *et al.* [26] calculated joint angular distributions (JADs) for two-photon DI by XUV pulses in both the nonsequential (39.5 eV $< \hbar\omega_{\rm XUV} <$ 54.4 eV) and the sequential ($\hbar\omega_{\rm XUV} >$ 54.4 eV) regimes for different energy sharings of the emitted electrons.

None of these theoretical investigations address the influence of an additional infrared (IR) laser on XUV double photoionization. The role of an assisting IR-laser pulse was studied by Hu in 2013 as a step toward the coherent control of chemical reactions [29]. The author's *ab initio* calculations for the DI of helium by an attosecond XUV pulse showed that the delay of the assisting few-cycle IR laser very sensitively influences the photoelectron energy distribution and can be tuned to significantly enhance the emission of fast photoelectrons. More recently, we have investigated few-photon DI of helium atoms without and in the presence of an assisting IR-laser field by numerically solving the time-dependent Schrödinger equation in full dimensionality [30]. These calculations were performed for the special case of equal energy sharing of the emitted electrons and focused on JADs generated by the absorption of a few XUV photons and the exchange of a specified effective number of IR photons with the assisting laser pulse.

In the present investigation, we extend our previous calculations to discuss the dependence of JADs on the energy sharing between the emitted electrons in laser-assisted single-XUV-photon DI. We consider the absorption of one ($\hbar\omega_{\rm XUV} =$ 89–99 eV) or two ($\hbar\omega_{\rm XUV} =$ 45 eV) XUV photons and compare the XUV-pulse-induced DI of helium without and with the assistance of an IR pulse. We discuss numerical examples for which the electrons are emitted from the ground state of helium with excess energies between 10 and 20 eV and find that the presence of the IR field alters photoelectron angular distributions in a characteristic way due to the transfer of photon momenta from the assisting IR pulse.

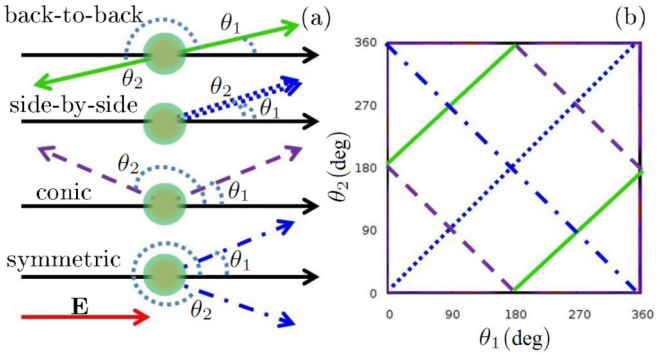

FIG. 1. (Color online) Schematics for (a) four different types of coplanar photoelectron emission patterns for the double ionization of helium: back-to-back emission, side-by-side emission, conic emission, and symmetric emission. (b) Corresponding main features in the joint angular distributions indicated by matching line styles and colors (See text).

This paper focusses on photoelectron angular distributions for coplanar emission. For this emission geometry, Fig. 1(a) distinguishes four typical electron emission types and defines the electron-emission angles, θ_i $(i = 1,2)$, relative to the (assumed equal) polarization directions of the XUV and IR pulses. The red solid arrow indicates the polarization direction of the XUV and IR electric fields. The remaining arrows indicate the asymptotic emission directions of the photoelectrons. Figure 1(b) shows schematically the main signatures of these emission types in JADs. Different colors and line styles in Figs. 1(a) and 1(b) correspond to the following distinguished emission patterns: (1) *back-to-back emission* (green solid lines with slope 45°). This pattern is forbidden by selection rules for single-photon DI and equal energy sharing; (2) *side-by-side emission* (blue dotted line along the diagonal $\theta_1 = \theta_2$). Side-by-side emission is forbidden at equal energy sharing due to the Coulomb repulsion of the emitted electrons; (3) *Conic emission* (purple dashed lines with slope −45°; and (4) *Symmetric emission* (blue dotted-dashed line along the diagonal given by $\theta_1 + \theta_2 = 360°$). At equal energy sharing of the emitted electrons, the symmetric emission pattern is dominant in single-photon DI, subject to selection rules [11,14].

We organize this paper as follows: In Sec. II we outline the theoretical method and its numerical implementation. In Sec. III, we discuss calculated JADs for few-XUV-photon DI of helium. Section IV contains numerical results for and a discussion of single-XUV-photon DI in the presence of short IR pulses, followed by our conclusions in Sec. V. Unless stated otherwise, we use atomic units throughout this paper. Based on extensive convergence tests [30], we performed all numerical calculations with the maximal total angular momentum quantum number $L = 5$ and maximal individual angular momentum quantum numbers for each electron $l = 5$.

II. THEORY AND NUMERICAL IMPLEMENTATION

In this section we briefly summarize the *ab initio* numerical method on which all results discussed in this work are based. A more comprehensive account of our implementation of the finite-element (FE) discrete-variable-representation method (DVR) and Arnoldi-Lanczos time-propagation scheme for solving the time-dependent Schrödinger equation (TDSE),

$$i\frac{\partial\Phi(\mathbf{r}_1,\mathbf{r}_2;t)}{\partial t} = H\Phi(\mathbf{r}_1,\mathbf{r}_2;t), \tag{1}$$

in full dimensionality for two-electron atoms can be found in Ref. [30], and references cited therein.

The correlated motion of the two helium electrons, subject to intra-atomic and time-dependent external-field interactions, is determined by the Hamiltonian $H = H_A + V_I$. The atomic Hamiltonian,

$$H_A = H_1 + H_2 + H_{\rm ee}, \tag{2}$$

consists of the hydrogenic Hamiltonians, $H_i = -\nabla_i^2/2 - Z/r_i$, $(i = 1,2)$, for the uncorrelated motion of each electron in the Coulomb field of the atomic nucleus with charge $Z = 2$ and the Coulomb interaction between the electrons $H_{\rm ee} = 1/|\mathbf{r}_1 - \mathbf{r}_2|$. The coupling of the electronic motion to the electric fields of the XUV and IR pulses in the dipole length gauge is given by

$$V_I = -[\mathbf{E}_{\rm XUV}(t) + \mathbf{E}_{\rm IR}(t)](\mathbf{r}_1 + \mathbf{r}_2). \tag{3}$$

We assume the XUV and IR pulses to be linearly polarized with sine-squared temporal profiles and write their electric-field vectors as

$$\mathbf{E}_a(t) = \begin{cases} \mathbf{E}_{0a}\sin^2\left(\frac{\pi t}{\tau_a}\right)\cos(\omega_a t + \varphi_a), & \text{if } 0 < t < \tau_a \\ 0, & \text{else,} \end{cases} \tag{4}$$

where the index a stands for XUV or IR. Their common polarization direction defines our quantization axis, which coincides with the z axis of our coordinate system. $|\mathbf{E}_{0a}|$, τ_a, φ_a, and ω_a denote electric-field amplitudes, pulse lengths, carrier-envelope phases, and frequencies, respectively. In this work we assume that the two pulses coincide and set $\varphi_{\rm XUV} = \varphi_{\rm IR} = 0$.

We expand the wave function of the IR- and XUV-field-driven two-electron atom,

$$\Phi(\mathbf{r}_1,\mathbf{r}_2;t) = \sum_{LM}\sum_{l_1,l_2}\frac{\psi_{l_1l_2}^{(LM)}(r_1,r_2;t)}{r_1r_2}\mathcal{Y}_{l_1l_2}^{L,M}(\hat{\mathbf{r}}_1,\hat{\mathbf{r}}_2), \tag{5}$$

in bipolar spherical harmonics,

$$\mathcal{Y}_{l_1l_2}^{LM}(\hat{\mathbf{r}}_1,\hat{\mathbf{r}}_2) = \sum_{m_1m_2} C_{l_1m_1l_2m_2}^{LM}Y_{l_1m_1}(\hat{\mathbf{r}}_1)Y_{l_2m_2}(\hat{\mathbf{r}}_2). \tag{6}$$

These express the coupling of the two electrons' individual angular momenta, specified by the quantum numbers l_i and m_i $(i = 1,2)$, in terms of ordinary spherical harmonics $Y_{l_im_i}(\hat{\mathbf{r}}_i)$ and Clebsch-Gordan coefficients $C_{l_1m_1l_2m_2}^{LM}$. The latter vanish, unless $|l_1 - l_2| \leqslant L \leqslant l_1 + l_2$ and $M = m_1 + m_2$. In the absence of external fields, the total angular momentum of the helium atom, defined by the quantum numbers L and M, is conserved and two-electron states for different (L,M) values [(L,M) symmetries] do not mix.

We calculate the evolution of the laser-driven helium atom wave function out of its $^1S_0$ ground state. For this singlet-spin state, the indistinguishability of the two Fermions requests symmetrical spatial wave function, $\Phi_{^1S_0}(\mathbf{r}_1,\mathbf{r}_2;t) = \Phi_{^1S_0}(\mathbf{r}_2,\mathbf{r}_1;t)$, such that the sum over L in Eq. (5) is limited to even values of $L - l_1 - l_2$. In addition, due to linear external-field polarizations along the z axis, only terms with

$M = 0$ contribute. We compute the initial singlet-spin state of helium using numerical imaginary-time propagation by replacing the real time t in the TDSE with the imaginary time $\tau = it$, starting with the product of Gaussian wave packets $Ce^{-(r_1-r_0)^2-(r_2-r_0)^2}$, where C is the normalization factor and $r_0 = 10$ [30,31].

The exact quantum-mechanical probability amplitude for detecting photoelectrons with momenta $\mathbf{k}_1$ and $\mathbf{k}_2$ is given as the projection of $\Phi(\mathbf{r}_1,\mathbf{r}_2;t_f)$ onto the asymptotic wave function for the two emitted electrons subject to their mutual Coulomb repulsion and attraction to the helium nucleus [32] after propagation of the two-electron wave function for a sufficiently long propagation time t_f. Since no closed-form expression is known for this asymptotic wave function of three Coulomb interacting particles, we calculate the probability amplitude by approximating the asymptotic two-electron wave function as the symmetrized product of Coulomb continuum wave functions $\psi^{(-)}_{\mathbf{k}_i}(\mathbf{r}_i)$, $i = 1,2$ that satisfy incoming-wave boundary conditions [33] in the unscreened electric field of the nuclear charge $Z = 2$,

$$\psi^{(-)}_{\mathbf{k}_1,\mathbf{k}_1} \approx \frac{1}{\sqrt{2}}\left[\psi^{(-)}_{\mathbf{k}_1}(\mathbf{r}_1)\psi^{(-)}_{\mathbf{k}_2}(\mathbf{r}_2) + \psi^{(-)}_{\mathbf{k}_2}(\mathbf{r}_1)\psi^{(-)}_{\mathbf{k}_1}(\mathbf{r}_2)\right]. \quad (7)$$

In order to the remove spurious contributions to the DI probability amplitude that are due to the nonorthogonality of this approximate asymptotic wave function and the initial state $\Phi_{^1S_0}$, we subtract the overlap with $\Phi_{^1S_0}(\mathbf{r}_1,\mathbf{r}_2)$ from $\Phi(\mathbf{r}_1,\mathbf{r}_2;t_f)$ to yield

$$\tilde{\Phi}(\mathbf{r}_1,\mathbf{r}_2;t) = \Phi(\mathbf{r}_1,\mathbf{r}_2;t) - \left\langle\Phi_{^1S_0}|\Phi(t)\right\rangle\Phi_{^1S_0}(\mathbf{r}_1,\mathbf{r}_2). \quad (8)$$

Numerical propagation of $\Phi(\mathbf{r}_1,\mathbf{r}_2;t)$ then allows us to compute the DI probability,

$$P(\mathbf{k}_1,\mathbf{k}_2) = \left|\left\langle\psi^{(-)}_{\mathbf{k}_1,\mathbf{k}_1}\middle|\tilde{\Phi}(\mathbf{r}_1,\mathbf{r}_2;t_f)\right\rangle\right|^2, \quad (9)$$

for detecting photoelectrons with momenta $\mathbf{k}_1$ and $\mathbf{k}_2$ [19,30] as a six-dimensional distribution in the momentum magnitudes k_1 and k_2 and corresponding momentum directions $\Omega_i = \hat{\mathbf{k}}_i = (\theta_i,\phi_i)$, $(i = 1,2)$. Integration over all angles results in the correlated energy distribution,

$$P(E_1,E_2) = \frac{1}{k_1k_2}\int d\Omega_1 d\Omega_2 P(\mathbf{k}_1,\mathbf{k}_2), \quad (10)$$

where $E_1 = k_1^2/2$ and $E_2 = k_2^2/2$ are the final (asymptotic) energies of the emitted electrons.

In numerical tests for equal energy sharing, $E_1 = E_2$, we found that external-field-free propagation for the time $T_f = 40$ after the end of the electric-field pulse is sufficient for obtaining correlated energy and angular distributions that are either converged or very close to convergence in the propagation time t_f [30]. For nonequal energy sharing, electron correlation in the final state tends to be less important than for equal energy sharing. By free propagation to $T_f = 40$ we therefore expect the calculated energy and angular distributions at nonequal energy sharing discussed in this work to be accurate within the error limits in typical double-ionization experiments [6].

III. ONE- AND TWO-XUV-PHOTON DOUBLE IONIZATION

In this section we discuss the DI of helium by either one or two XUV photons ($N_{\mathrm{XUV}} = 1,2$) without an assisting IR-laser pulse (Fig. 2). The small number of absorbed XUV photons and specific energy sharing enable us to first clearly expose the emission mechanism and symmetry constraints imposed by selection rules, before discussing angular distributions for laser-assisted XUV DI in Sec. IV. All numerical results in this section and in Sec. IV are calculated for coplanar emission where $\phi_1 = \phi_2 = 0$. We consider sine-squared XUV pulses as given by Eq. (4) with a peak intensity of $I_0 = 10^{14}$ W/cm^2, durations of 1 fs, corresponding to a spectral width (full width-half maximum in intensity) of $\hbar\Delta\omega_{\mathrm{XUV}} \approx 6$ eV and photon energies at the pulses' spectral centers of $\hbar\omega_{\mathrm{XUV}} = 45$, 90, and 99 eV.

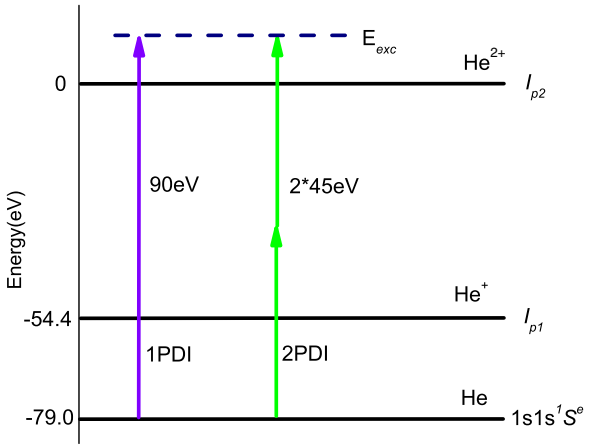

FIG. 2. (Color online) Energetics for nonsequential double ionization of helium by two 45 or one 90 eV photons. I_{p_1} and I_{p_2} designate the first and second ionization threshold, respectively, leading a combined excess energy of the emitted electrons of $E_{\mathrm{exc}} = E_1 + E_2 = 11$ eV.

A. Triply differential cross sections

Integration of Eq. (9) over k_2 (or k_1) leads to the TDCS [19,26]:

$$\frac{d^3\sigma}{dE_1 d\Omega_1 d\Omega_2} = \left(\frac{\omega}{I_0}\right)^2 \frac{k_1}{T_{\mathrm{eff}}}\int dk_2 k_2^2 P(\mathbf{k}_1,\mathbf{k}_2). \quad (11)$$

The TDCS is defined in terms of the effective interaction time,

$$T_{\mathrm{eff}} = \int dt\left(\frac{I(t)}{I_0}\right)^{N_{\mathrm{XUV}}}, \quad (12)$$

for a given number N_{XUV} of absorbed XUV photons and XUV intensity profile $I(t)$. For a sine-squared pulse, $T_{\mathrm{eff}} = 3/8\tau_{\mathrm{XUV}}$, if $N_{\mathrm{XUV}} = 1$, and $T_{\mathrm{eff}} = 35/128\tau_{\mathrm{XUV}}$, if $N_{\mathrm{XUV}} = 2$.

Figure 3 shows the TDCSs according to Eq. (11) for $\hbar\omega_{\mathrm{XUV}} = 99$ eV and detection of one electron at fixed angles $\theta_1 = 0^\circ$, 30°, and 60° relative to the XUV-pulse polarization direction as a function of the other electron's emission angle θ_2. Our calculated conditional TDCSs for coplanar emission are in good agreement with measured absolute conditional angular distributions [6,34]. For $\theta_1 = 0^\circ$, our TDCSs for equal energy sharing [Fig. 3(a)] and unequal energy sharing [Fig. 3(b)] are

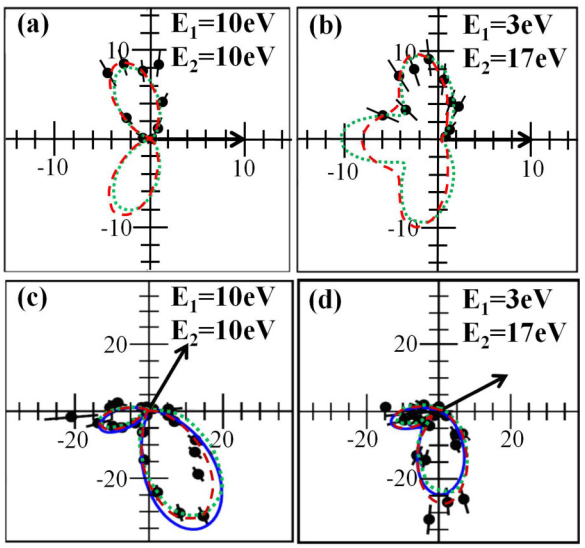

FIG. 3. (Color online) TDCSs in units of $beV^{-1}sr^{-2}$ for the double ionization of helium and fixed detection angles (a, b) $\theta_1 = 0°$, (c) 60°, and (d) 30°, indicated by the back arrows. The central XUV-photon energy is 99 eV. The black dots with error bars are absolute experimental TDCSs from Ref. [6]. Our calculated results are shown as red dashed lines and normalized to the experimental data at (a) $\theta_2 = 110°$, (b) 95°, (c) 295°, and (d) 275°. (a, c) Equal energy sharing with $E_1 = E_2 = 10$ eV ($\varepsilon = 0.5$). (b, d) Unequal energy sharing with $E_1 = 3$ eV ($\varepsilon = 0.15$). The green dotted lines show theoretical results of (a) Huetz *et al.* [6,10] and (b–d) Kheifets and Bray [6]. (c, d) The solid blue lines show TDCC results of Palacios *et al.* [15].

symmetrical about the XUV polarization direction, as expected from symmetry considerations.

For $\theta_1 = 0°$ and equal energy sharing with $E_1 = E_2 =$ 10 eV, the dominant angular difference $|\theta_2 - \theta_1|$ between the two electrons is $\Theta_{12} \approx 130°$ [Fig. 3(a)]. In compliance with known selection rules for DI at equal energy sharing [1,13], side-by-side and back-to-back emission are prohibited. This graph also shows good agreement of our calculation with the theoretical results of Huetz *et al.* [6,10].

The conditional TDCSs at fixed $\theta_1 = 0°$ in Fig. 3(b) for nonequal energy sharing with $E_1 = 3$ eV and $E_2 = 17$ eV, corresponding to the energy-sharing parameter,

$$\varepsilon = \min\left\{\frac{E_1}{E_1+E_2}, \frac{E_2}{E_1+E_2}\right\} = 0.15, \tag{13}$$

reveal preferred angular differences Θ_{12} equal to ≈130° and 180°. Back-to-back emission now occurs, while side-by-side emission remains prohibited as for the case of equal energy sharing [1,13]. Figures 3(b)–3(d) include the results of a comparison with the theoretical CCC results of Kheifets and Bray [6]. Figures 3(c) and 3(d) compare CCC results of Kheifets and Bray [6], TDCC calculations by Palacios *et al.* [15], and our calculations for equal [Fig. 3(c)] and nonequal energy sharing with $\varepsilon = 0.15$ [Fig. 3(d)] for fixed emission angles $\theta_1 = 60°$ and 30°, respectively.

As for Figs. 3(a) and 3(b), the dominant angular difference Θ_{12} in Figs. 3(c) and 3(d) is ≈130°. The comparison of the conditional TDCSs at different energy sharings shown in Figs. 3(a)–3(d) suggests the interpretation of Θ_{12} as a measure for the relevance of electronic correlation for DI, larger values of Θ_{12} indicating a more prominent role of electronic correlation. We numerically verified that $\Theta_{12} \approx 130°$ for arbitrary emission angles θ_1, not just for the special cases $\theta_1 = 0°$ and 60°. For the excess energy we consider in this section (20 eV), our results for Θ_{12} agree with the theoretical prediction of Jiang *et al.* [28]. The dominant relative emission angle Θ_{12} thus characterizes the DI process regardless of any conditions imposed on θ_1.

B. Joint angular distributions

Based on the DI probability distribution Eq. (9), the JAD for DI in coplanar geometry as a function of the energy sharing ε between the emitted electrons and emission angles relative to the laser polarization can be written as [26]:

$$P(\theta_1,\theta_2;\varepsilon) = \sum_{i=1}^{2}\int dk_1 dk_2 \frac{k_1^2 k_2^2}{2}\delta\left(\varepsilon - \frac{E_i}{E_1+E_2}\right)P(\mathbf{k}_1,\mathbf{k}_2). \tag{14}$$

For equal energy sharing and sufficiently long XUV pulses, the TDCS Eq. (11) is proportional to the JAD.

Based on angular-momentum algebra, Huetz *et al.* [10] showed that the DI probability Eq. (9) can be written as the square of the sum of two terms, where each terms is the product of an angular factor and a complex-valued amplitude,

$$P(\mathbf{k}_1,\mathbf{k}_2) \sim |a_s(E_1,E_2,\theta_{12})[\cos(\theta_1)+\cos(\theta_2)] + a_a(E_1,E_2,\theta_{12})[\cos(\theta_1)-\cos(\theta_2)]|^2. \tag{15}$$

The amplitudes a_s and a_a are symmetric and antisymmetric under the exchange of E_1 and E_2, respectively, and depend on the difference angle:

$$\theta_{12} = \begin{cases}\theta_2 - \theta_1, & \text{if } \theta_1 < \theta_2\\ \theta_2 - \theta_1 + 2\pi, & \text{if } \theta_1 > \theta_2.\end{cases} \tag{16}$$

For the special case of equal energy sharing, the antisymmetric term vanishes, and the DI probability consists of a coherent sum of dipole distributions in θ_1 and θ_2 that is modified by the correlation factor $|a_s|^2$. Inspired by Wannier theory for near-threshold DI, writing this factor as a Gaussian function with an angle-independent scaling factor $b(E)$ [35],

$$|a_s|^2 = b(E)\exp\left\{-2ln2\left[\frac{\theta_{12}-\pi}{\theta_{1/2}}\right]^2\right\}, \tag{17}$$

the adjustment of a single parameter $\theta_{1/2}$ provides a good fit to measured DI distributions, even at photon energies far beyond the near-threshold region [10]. The width of the angular distribution $\theta_{1/2}$ is a measure for the importance of electronic correlation, in analogy to the dominant angle Θ_{12} identified in the TDCS discussed in the preceding subsection. For increasingly unequal energy sharing the antisymmetric term in Eq. (15) increases, allowing for back-to-back emission.

Figures 4(a)–4(c) show calculated JADs for single-photon DI at a central XUV-photon energy of 90 eV. All JADs in Figs. 4(a)–4(c) and 5(a)–5(c) are normalized to their maxima

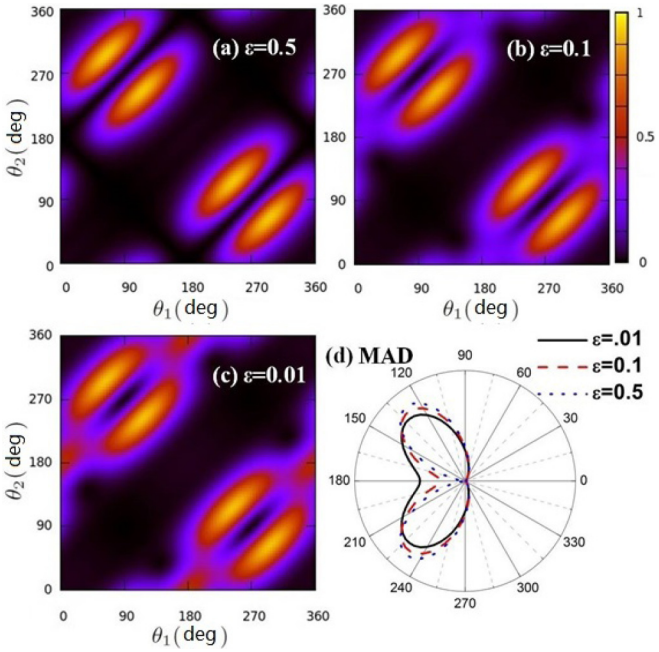

FIG. 4. (Color online) Calculated normalized joint angular distributions for the double ionization of helium by one $\hbar\omega_{\mathrm{XUV}} = 90$ eV XUV photon at (a) equal energy sharing ($\varepsilon = 0.5$), (b) unequal energy sharing ($\varepsilon = 0.1$), and (c) extremely unequal energy sharing ($\varepsilon = 0.01$). (d) Mutual angular distributions extracted from (a–c), displaying the angular distributions versus the angular difference θ_{12} of the emitted electrons, Eq. (16). The XUV pulse has a peak intensity of 10^{14} W/cm^2 and pulse length of 1 fs.

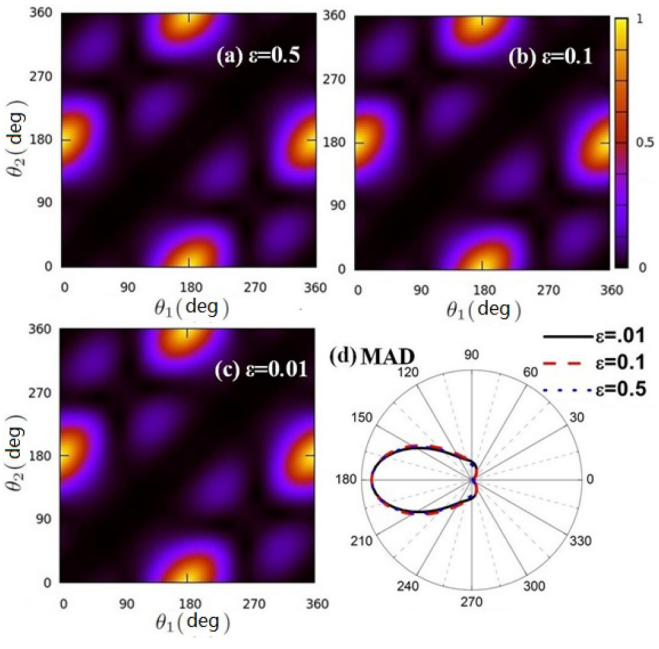

FIG. 5. (Color online) Calculated normalized joint angular distributions for the double ionization of helium by two $\hbar\omega_{\mathrm{XUV}} = 45$ eV XUV photons at (a) equal energy sharing ($\varepsilon = 0.5$), (b) unequal energy sharing ($\varepsilon = 0.1$), and (c) extremely unequal energy sharing ($\varepsilon = 0.01$). (d) Mutual angular distributions extracted from (a–c). The XUV pulse has a peak intensity of 10^{14} W/cm^2 and a pulse length of 1 fs. For two-photon DI, the angular distributions are insensitive to changes in the energy sharing.

and their yields are plotted on a linear scale. Going from equal energy sharing in Fig. 4(a) to unequal energy sharing with $\varepsilon = 0.1$ [Fig. 4(b)] and extremely unequal energy sharing with $\varepsilon = 0.01$ [Fig. 4(c)], symmetric emission remains dominant, while back-to-back emission is fading in to compete with symmetric emission for $\varepsilon = 0.01$, as suggested by Eq. (17).

Normalized calculated JADs for the DI of helium by two $\omega_{\mathrm{XUV}} = 45$ eV XUV photons are shown in Figs. 5(a)–5(c). The central XUV-photon energy and spectral profile of the 1 fs XUV pulses are in the photon energy range for nonsequential DI, 39.5 eV $< \hbar\omega_{\mathrm{XUV}} <$ 54.4 eV, excluding contributions due to sequential DI. After the absorption of two photons, the final state of the three-particle system has even parity, the total angular-momentum quantum number L being equal to either 0 or 2. In contrast to single-photon DI, where the odd final-state parity prohibits back-to-back emission for equal energy sharing, both equal and unequal energy sharing are subject to the same selection rules [11]. Back-to-back emission is now allowed for any energy sharing of the photoelectrons. As a result of the double electron-emission process depending on electronic correlation and the lack of censorship imposed by selection rules, unhindered electronic repulsion shapes the JADs. Accordingly, our JADs for equal energy sharing in Fig. 5(a), unequal energy sharing with $\varepsilon = 0.1$ [Fig. 5(b)], and extremely unequal energy sharing with $\varepsilon = 0.01$ [Fig. 5(c)] are insensitive to the energy sharing and dominated by back-to-back emission.

C. Mutual angular distributions

Integration of the JAD Eq. (14) over θ_1 (or θ_2) at fixed mutual angles θ_{12} defines the mutual angular distribution (MAD):

$$P(\theta_{12};\varepsilon) = \int d\theta_1 P(\theta_1, \theta_1 + \theta_{12}, \varepsilon). \tag{18}$$

Figures 4(d) and 5(d) show the MADs derived from the JADs shown in Figs. 4(a)–4(c) and 5(a)–5(c), respectively, separately normalized to the area inclosed in the polar plots.

The MADs in Fig. 4(d) clearly display the dependence of single-photon DI on the energy sharing, which is seen in the underlying JADs [Figs. 4(a)–4(c)]. The MADs show further that the photoelectrons are almost exclusively emitted in opposite half-spaces over a large range of energy sharing parameters ε. The curve for equal energy sharing $\varepsilon = 0.5$ conforms with the symmetry requirement of vanishing back-to-back and side-by-side emission, while back-to-back emission becomes more prominent for unequal ($\varepsilon = 0.1$) and extremely unequal $\varepsilon = 0.01$ energy sharing. For all energy sharings, side-by-side emission is absent and the dominant mutual angle is $\Theta_{12} \approx 130^\circ$. For equal energy sharing this agrees with the experimental data shown in the TDCS for a slightly higher photon energy in Fig. 3(a) above. At $\varepsilon = 0.01$ the yield at back-to-back emission is about 70% of the yield at $\theta_{12} = 130^\circ$.

The MADs for DI by two 45 eV photons in Fig. 5(d) show dominant back-to-back emission and two minor peaks at $\theta_{12} \approx 75^\circ$ and $\approx 285^\circ$. The minor peaks correspond to the four minor peaks for symmetrical emission seen along the negatively sloped diagonal lines in the underlying JADs in

Figs. 5(a)–5(c). The MADs also show almost no dependence on the energy sharing, as the JADs in Figs. 5(a)–5(c).

IV. LASER-ASSISTED SINGLE-XUV-PHOTON DOUBLE IONIZATION

We found in a previous study of the DI of helium at equal energy sharing that the addition of a comparatively weak IR field to the ionizing XUV pulse leads to the appearance of characteristic sidebands in energy and angle distributions [30]. In this section we extend these investigations to nonequal energy sharing. We analyze JADs and MADs for XUV pulses with 10^{14} W/cm^2 peak intensity, $\tau_{\rm XUV} = 1$ fs pulse duration, and $\hbar\omega_{\rm XUV} = 89$ eV central photon energy that coincide with an assisting IR pulse with a peak intensity of 3×10^{12} W/cm^2, pulse lengths $\tau_{\rm IR} = 2.6$ fs, and $\hbar\omega_{\rm IR} = 1.61$ eV photon energy, as given by Eq. (4).

We are going to compare angular distributions for equal and unequal energy sharing between the photoelectrons and distinguish contributions from even and odd effective numbers of photons involved for clarity. For even (odd) effective numbers we include one 89 eV XUV photon plus any odd (even) number of IR photons. We calculate these "even" and "odd" contributions to JADs and MADs by restricting the partial-wave expansion of the time-dependent wave function for the helium atom Eq. (5) in the combined XUV and IR fields to even and odd values of the total angular momentum quantum number L. We compute the angular distributions discussed below by integrating joint energy distributions across all sidebands (all possible energies E_1 and E_2) for a given value of the energy-sharing parameter ε.

A. Joint angular distributions

Figure 6 shows our calculated JADs for laser-assisted single-XUV-photon DI for odd and even effective photon numbers in the top panel and bottom panel, respectively, for three different energy sharings. Even though side-by-side emission is possible at unequal energy sharing, no relevant contribution can be seen on the linear-scale graphs, regardless of the final-state parity.

For odd effective photon numbers (odd parity final states), the equal energy-sharing distributions in Figs. 6(a)–6(c) have kept the four symmetrical-emission peaks, which are the main features of single-photon DI without an assisting IR field [cf. Fig. 4]. As the energy symmetry is broken, symmetrical emission remains dominant at $\varepsilon = 0.1$ [Fig. 6(b)] and small contribution from back-to-back emission emerge, as for the laser-free single-XUV-photon DI [cf. Fig. 4(b)]. For extremely unequal energy sharing at $\varepsilon = 0.01$ [Fig. 6 (c)], both symmetric and back-to-back emission are prominent in the JAD. However, in contrast to laser-free DI [cf. Fig. 4(c)], the peak DI yield for back-to-back exceeds the peak yields for symmetric emission. For odd parity final states and unequal energy sharing, a striking change induced by the assisting laser pulse is thus the promotion of back-to-back emission.

Contributions to the JAD from even effective photon numbers (even parity final states) show competing symmetrical and back-to-back emission over a large range of energy

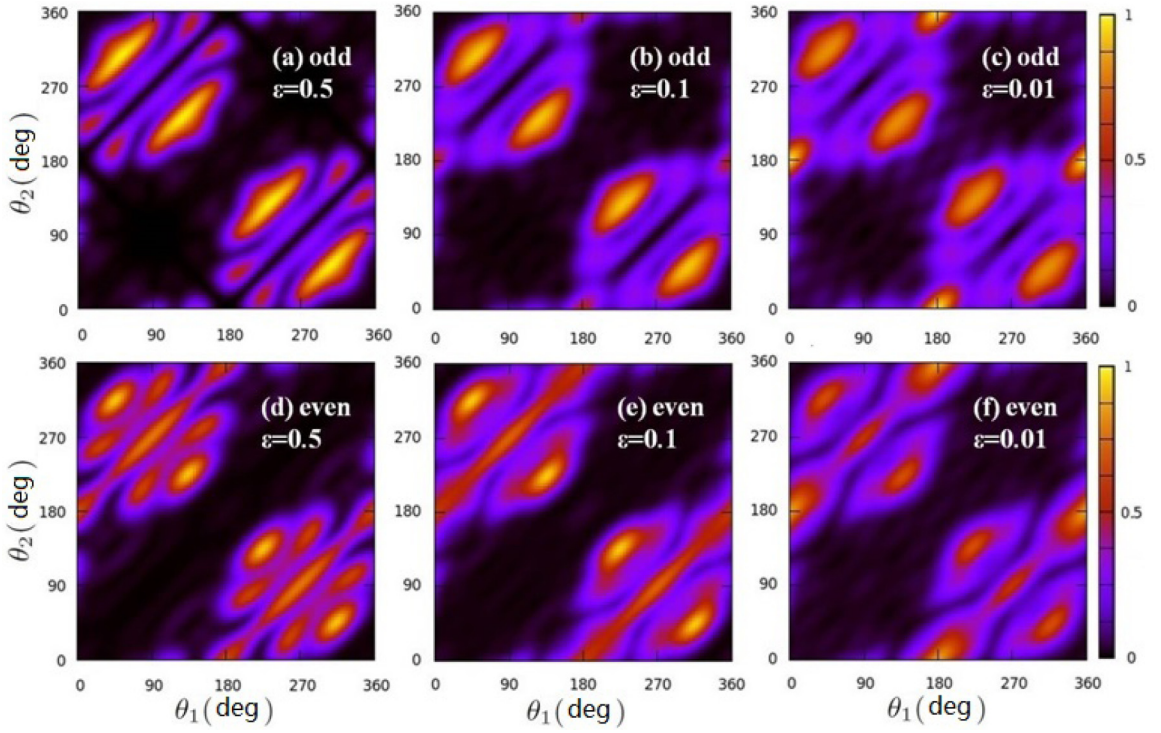

FIG. 6. (Color online) Calculated normalized joint angular distributions for IR laser-assisted single-XUV-photon double ionization of helium by 10^{14} W/cm^2 peak intensity $\hbar\omega_{\rm XUV} = 89$ eV XUV pulses assisted by coincident 3×10^{12} W/cm^2 IR-laser pulses. Contribution to the double-ionization yield from (a)–(c) odd and (d)–(f) even total effective numbers of XUV plus IR photons. Results for (a, d) equal energy sharing ($\varepsilon = 0.5$), (b, e) unequal energy sharing ($\varepsilon = 0.1$), and (c, f) extremely unequal energy sharing ($\varepsilon = 0.01$).

sharings. These main contributors to DI in Figs. 6(d)–6(f) are the same as for laser-free DI by two 45 eV photons [cf. Fig. 5], albeit with very different relative yields. Unlike laser-free even-parity DI by two 45 eV photons, our even-photon-number results in Figs. 6(d)–6(f) are sensitive to changes in the energy sharing. Interestingly, while at equal energy sharing back-to-back emission is strictly prohibited for single-photon DI, the absorption of an additional odd number of IR photons enables clearly noticeable back-to-back emission [Fig. 6(d)].

B. Mutual angular distributions

Figure 7 shows MADs for laser-assisted single-XUV-photon DI. All distributions are normalized to the enclosed area and extracted from the corresponding JADs shown in Fig. 6 according to Eq. (18).

For odd total effective numbers of XUV plus IR photons (odd parity), side-by-side ($\theta_{12} = 0°$) and back-to-back emission ($\theta_{12} = 180°$) are strictly forbidden at equal energy sharing [Fig. 7(a)]. For unequal energy sharing, both side-by-side and back-to-back emission (red dashed line) occur and become increasingly prominent with increasing energy asymmetry. For extremely unequal energy sharing ($\varepsilon = 0.01$), the back-to-back-emission yield reaches ≈80% of the peak value at $\Theta_{12} \approx 105°$, while the side-by-side-emission yield reaches ≈15% of the peak value.

For even parity back-to-back emission strongly dominates the MADs in Fig. 7(b), regardless of the energy sharing. The side-by-side-emission yields remain very small at unequal energy sharing ($\varepsilon = 0.1$) and are largest at extremely unequal energy sharing ($\varepsilon = 0.01$). The small but noticeable side-by-side-emission yield at $\varepsilon = 0.01$ is compatible with a two-step mechanism. This mechanism operates by the fast photoelectron carrying away almost the entire excess energy, while the slow electron reverses its motion by absorbing one IR photon to follow the fast electron. This picture thus explains noticeable side-by-side contributions by allowing the electrons to initially move in opposite directions, i.e., along the strongly favored back-to-back emission directions, while being compatible with dipole sections rules that would prohibit side-by-side emission without an assisting IR-laser pulse.

In order to more clearly display the enhancement of side-by-side and back-to-back emission by the assisting IR-laser pulse and to show this effect on observable MADs (including odd and even parity contributions), we compare in Fig. 8 MADs for single-XUV-photon DI of helium with and without the assisting IR-laser field at different energy sharings. To allow a quantitative comparison, the distributions in Fig. 8 are not individually normalized, in contrast to the MADs shown in Fig. 7.

This comparison shows that each peak in the MADs for IR-laser-free DI splits into two peaks in the presence of the weak IR-laser field. This splitting of the dominant emission angles is due to momentum transfers from the IR field. Absorbing equal amounts of energy from the IR field, photoelectrons released by the XUV field are thus pushed either toward the side-by-side or back-to-back emission direction. At equal energy sharing [Fig. 8(a)], this momentum transfer changes the dominant relative emission angle from $\Theta_{12} \approx 130°$ for IR-laser-free emission to ≈105° and ≈170° for IR-laser-assisted emission. For extremely unequal energy sharing [Fig. 8(b)], the dominant relative emission angle splits from ≈135° for IR-laser-free emission to ≈95° and ≈170° for IR-laser-assisted emission.

The dominant mutual angles for the even-parity contributions are ≈130° and ≈180° for equal, and ≈95° and ≈170° for extremely unequal energy sharing (Fig. 8). For odd parity final states the dominant relative angles can be estimated by vector addition. For equal energy sharing ($E_1 = E_2 = 5$ eV), the dominant photoelectron momentum vector (in plane polar coordinates), $(k_1, \Theta_{12}) = (0.606, 130°)$, changes upon absorption of an IR photon by approximately $\pm(A_{0,\mathrm{IR}}, 0)$, where $A_{0,\mathrm{IR}} \approx 0.156$ is the peak amplitude of the vector potential at 3×10^{12} W/cm^2 peak intensity of the IR pulse. This vector addition results in estimated dominant mutual angles for IR-laser-assisted emission of $\Theta_{12} = 106°$ and 159°, in good agreement with the numerical results in Fig. 8(a).

We note that for even parity (i.e., absorption of one XUV, assisted by an odd number of IR photons), the exchange of IR photons results in final states that include contributions

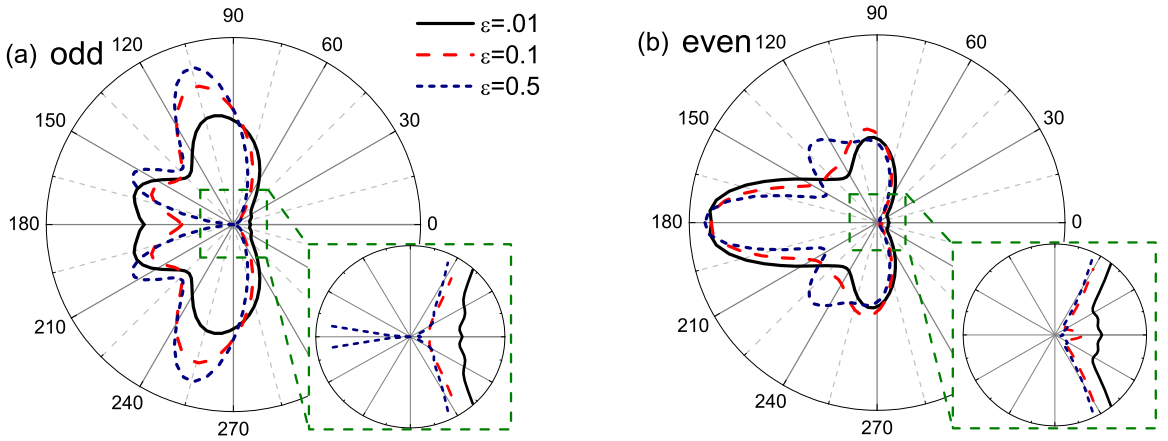

FIG. 7. (Color online) Mutual angular distributions for IR-laser-assisted single-XUV-photon double ionization of helium for different energy sharings ε. (a) Contributions to the double-ionization yield from (a) odd and (b) even total effective numbers of XUV plus IR photons. The XUV and IR pulse parameters are the same as described in the caption of Fig. 6. The insets zoom into the distributions near the mutual angles $\theta_{12} = 0°$.

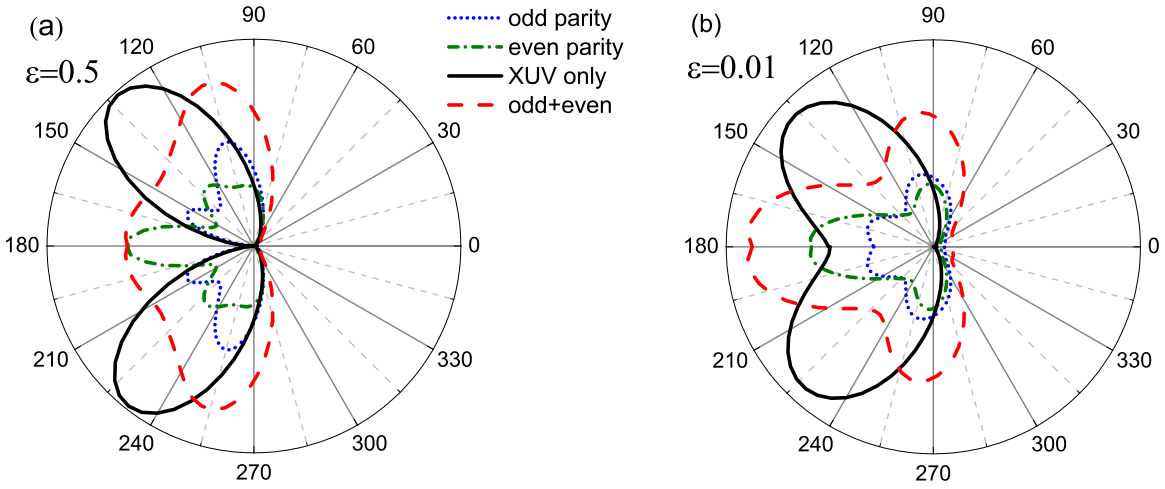

FIG. 8. (Color online) Contributions to the mutual angular distributions for IR-laser-assisted single-XUV-photon double ionization of helium for (a) equal energy sharing and (b) extremely unequal energy sharing with $\varepsilon = 0.01$. XUV- and IR-pulse parameters are the same as described in the caption of Fig. 6. The black solid curves correspond to XUV-pulse-only results, blue dotted lines to odd parity, and green dash-dotted lines display even parity. The red dashed curves show coherent additions of odd and even parity contributions.

from different total angular momenta, e.g., $L = 0,2$, if one IR photon is absorbed. Due to this coherent superposition of states with different symmetry, the simple addition of electron momenta and IR vector potential does not explain the dominant angles for even-parity contributions to laser-assisted XUV DI.

These IR-pulse-induced changes in photoelectron angular distributions illustrate known constraints imposed by dipole selection rules. They are robust over a large range of energy sharings between the emitted electrons, and, for special cases, can be classically estimated by simple vector addition, based on the transfer of IR-photon momenta to photoelectrons.

V. CONCLUSION

We analyzed the dependence of joint and mutual photoelectron angular distributions on the energy sharing of the emitted electrons for the DI of helium atoms by short XUV pulses in coplanar emission geometry with and without the presence of a comparatively weak IR-laser pulse. Compared to laser-free single-XUV-photon DI of helium, we found that the presence of a weak IR field can dramatically change the JAD of the two escaping electrons, leading to (i) angular shifts and a splitting into two dominant emission directions, (ii) strong enhancement of back-to-back emission at all energy sharings, and (iii) enhanced side-by-side emission yields at extremely unequal energy sharing.

ACKNOWLEDGMENTS

This work was supported by the United States National Science Foundation (NSF) under Grant No. PHY-1068752 and the Division of Chemical Sciences, Office of Basic Energy Sciences, Office of Energy Research, U.S. Department of Energy. Part of this research used computational resources of (i) the National Energy Research Scientific Computing Center, which is supported by the Office of Science of the U.S. Department of Energy under Contract No. DE-AC02-05CH11231 and (ii) the Beocat Research Cluster at Kansas State University, which is funded in part by NSF Grants No. CNS-1006860, No. EPS-1006860, and No. EPS-0919443.

[1] J. S. Briggs and V. Schmidt, J. Phys. B: Atom. Mol. Opt. Phys. **33**, R1 (2000).
[2] C. W. McCurdy, M. Baertschy, and T. N. Rescigno, J. Phys. B: Atom. Mol. Opt. Phys. **37**, R137 (2004).
[3] O. Schwarzkopf, B. Krässig, J. Elmiger, and V. Schmidt, Phys. Rev. Lett. **70**, 3008 (1993).
[4] O. Schwarzkopf and V. Schmidt, J. Phys. B: Atom. Mol. Opt. Phys. **28**, 2847 (1995).
[5] O. Schwarzkopf and V. Schmidt, J. Phys. B: Atom. Mol. Opt. Phys. **29**, 1877 (1996).
[6] H. Bräuning, R. Dörner, C. L. Cocke, M. H. Prior, B. Krässig, A. S. Kheifets, I. Bray, A. Bräuning-Demian, K. Carnes, S. Dreuil, V. Mergel, P. Richard, J. Ullrich, and H. Schmidt-Böcking, J. Phys. B: Atom. Mol. Opt. Phys. **31**, 5149 (1998).
[7] H. Hasegawa, E. J. Takahashi, Y. Nabekawa, K. L. Ishikawa, and K. Midorikawa, Phys. Rev. A **71**, 023407 (2005).
[8] G. H. Wannier, Phys. Rev. **90**, 817 (1953).
[9] J. M. Feagin, J. Phys. B: Atom. Mol. Opt. Phys. **17**, 2433 (1984).
[10] A. Huetz, P. Selles, D. Waymel, and J. Mazeau, J. Phys. B: Atom. Mol. Opt. Phys. **24**, 1917 (1991).
[11] F. Maulbetsch and J. S. Briggs, J. Phys. B: Atom. Mol. Opt. Phys. **26**, 1679 (1993).
[12] F. Maulbetsch and J. S. Briggs, J. Phys. B: Atom. Mol. Opt. Phys. **27**, 4095 (1994).
[13] F. Maulbetsch and J. S. Briggs, J. Phys. B: Atom. Mol. Opt. Phys. **28**, 551 (1995).
[14] F. Maulbetsch, M. Pont, J. S. Briggs, and R. Shakeshaft, J. Phys. B: Atom. Mol. Opt. Phys. **28**, L341 (1995).

[15] A. Palacios, T. N. Rescigno, and C. W. McCurdy, Phys. Rev. A **77**, 032716 (2008).
[16] J. S. Parker, L. R. Moore, K. J. Meharg, D. Dundas, and K. T. Taylor, J. Phys. B: Atom. Mol. Opt. Phys. **34**, L69 (2001).
[17] A. S. Kheifets and I. A. Ivanov, J. Phys. B: Atom. Mol. Opt. Phys. **39**, 1731 (2006).
[18] D. A. Horner, F. Morales, T. N. Rescigno, F. Martín, and C. W. McCurdy, Phys. Rev. A **76**, 030701(R) (2007).
[19] X. Guan, K. Bartschat, and B. I. Schneider, Phys. Rev. A **77**, 043421 (2008).
[20] A. Palacios, T. N. Rescigno, and C. W. McCurdy, Phys. Rev. A **79**, 033402 (2009).
[21] A. Palacios, T. N. Rescigno, and C. W. McCurdy, Phys. Rev. Lett. **103**, 253001 (2009).
[22] A. Palacios, D. A. Horner, T. N. Rescigno, and C. W. McCurdy, J. Phys. B: Atom. Mol. Opt. Phys. **43**, 194003 (2010).
[23] M. Førre, S. Selstø, and R. Nepstad, Phys. Rev. Lett. **105**, 163001 (2010).
[24] S. A. Sørngård, S. Askeland, R. Nepstad, and M. Førre, Phys. Rev. A **83**, 033414 (2011).
[25] H. Bachau, Phys. Rev. A **83**, 033403 (2011).
[26] Z. Zhang, L. Y. Peng, M. H. Xu, A. F. Starace, T. Morishita, and Q. Gong, Phys. Rev. A **84**, 043409 (2011).
[27] L. Y. Peng, Z. Zhang, W. C. Jiang, G. Q. Zhang, and Q. Gong, Phys. Rev. A **86**, 063401 (2012).
[28] W. C. Jiang, L. Y. Peng, W. H. Xiong, and Q. Gong, Phys. Rev. A **88**, 023410 (2013).
[29] S. X. Hu, Phys. Rev. Lett. **111**, 123003 (2013).
[30] A. Liu and U. Thumm, Phys. Rev. A **89**, 063423 (2014).
[31] S. X. Hu, Phys. Rev. E **81**, 056705 (2010).
[32] M. Brauner, J. S. Briggs, and H. Klar, J. Phys. B: Atom. Mol. Opt. Phys. **22**, 2265 (1989).
[33] A. R. Barnett, in *Computational Atomic Physics*, edited by K. Bartschat (Springer, Heidelberg/New York, 1996), Chap. 9, p. 181.
[34] O. Schwarzkopf, B. Krässig, and V. Schmidt, J. Phys. **3**, 169 (1993); O. Schwarzkopf, Ph.D. thesis, University of Freiburg, Germany, 1995.
[35] L. Avaldi and A. Huetz, J. Phys. B: Atom. Mol. Opt. Phys. **38**, S861 (2005).